

# Giant quenching and mobile-carrier-assisted recovery of ordered moments in $\text{La}_{0.7}\text{Ca}_{0.3}\text{MnO}_3/\text{Er}_{0.7}\text{Sr}_{0.3}\text{MnO}_3$ and $\text{La}_{0.7}\text{Ca}_{0.3}\text{MnO}_3/\text{LaNiO}_3$ superlattices

Prahallad Padhan and R. C. Budhani

*Department of Physics, Indian Institute of Technology Kanpur, Kanpur-208016, India*

(Received 10 May 2004; published 21 April 2005)

We report measurements of magnetic ordering temperature, magnetic moment, and resistivity of  $\text{La}_{0.7}\text{Ca}_{0.3}\text{MnO}_3/\text{LaNiO}_3$  and  $\text{La}_{0.7}\text{Ca}_{0.3}\text{MnO}_3/\text{Er}_{0.7}\text{Sr}_{0.3}\text{MnO}_3$ , thin film superlattices. The ordered moment per Mn ion of the ferromagnetic layers undergoes a giant quenching as the insulating spacer layer ( $\text{Er}_{0.7}\text{Sr}_{0.3}\text{MnO}_3$ ) thickness is increased. We attribute the quenching to random pinning of the  $t_{2g}$  spins of Mn ions in a disordered interfacial zone of length scale  $\lambda_c$ . The nonzero quenching followed by full recovery seen at large  $n$  in superlattices with the metallic spacer ( $\text{LaNiO}_3$ ), suggest a mobile-carrier-assisted depinning of the  $t_{2g}$  spins in the disordered zone.

DOI: 10.1103/PhysRevB.71.144415

PACS number(s): 75.70.Cn, 75.47.Gk, 75.47.Lx

Thin film multilayers of  $3d$ ,  $4d$ , and  $4f$  series metals have been a topic of active research for many decades. A variety of fascinating phenomena have been observed in such synthetic periodic structures.<sup>1-3</sup> With the discovery of high  $T_c$  superconductivity and colossal magnetoresistance in doped transition metal oxides, research is now focused on periodic structures of the doped oxides.<sup>4-18</sup> Amongst these, the superlattices where thin layers of a ferromagnetic (FM) manganite are separated by a nonmagnetic oxide of metallic, superconducting or insulating character are of particular attention. The fundamental interest here is to understand the long-range magnetic ordering across nonmagnetic spacers, and the coexistence of ferromagnetism and superconductivity. Technologically, spin polarized transport and large magnetoresistance are potentially accessible at room temperature and low magnetic fields in oxide-based systems.

As in the case of  $3d$  transition metal superlattices,<sup>3,19</sup> signatures of oscillatory exchange coupling have been seen in some multilayers of manganites.<sup>14,18</sup> However, the magnetotransport and magnetic coupling in these systems are sensitive to the stereochemical distortions in the coordination of magnetic ions at the interfaces. For example, Izumi *et al.*<sup>7</sup> have observed a large quenching of the magnetic moment per Mn site in  $\text{La}_{0.6}\text{Sr}_{0.4}\text{MnO}_3/\text{La}_{0.6}\text{Sr}_{0.4}\text{FeO}_3$  multilayers where the Fe-based perovskite is a  $G$ -type antiferromagnetic (AF) insulator. These authors attribute the suppression of the moment to frustration of Mn spins at the interfaces due to their proximity to the  $G$ -type AF spin arrangement. Measurements by the same group on  $\text{La}_{0.6}\text{Sr}_{0.4}\text{MnO}_3/\text{La}_{0.45}\text{Sr}_{0.55}\text{MnO}_3$ , where the Sr-rich spacer compound is an  $A$ -type metallic antiferromagnet, do not show any suppression of the moment.<sup>11</sup> While there is a large difference in the electrical conductivity of the spacers  $\text{La}_{0.45}\text{Sr}_{0.55}\text{MnO}_3$  and  $\text{La}_{0.6}\text{Sr}_{0.4}\text{FeO}_3$ , Izumi *et al.*<sup>7,11</sup> attribute the drop in the moment only to the  $G$ -type spin arrangement. However, a similar quenching of the moments is also observed in superlattices where the ferromagnetic layers of  $\text{La}_{0.6}\text{Sr}_{0.4}\text{MnO}_3$  or  $\text{La}_{0.7}\text{Ca}_{0.3}\text{MnO}_3$  are separated by an insulator such as  $\text{SrTiO}_3$ , which does not show any magnetic ordering.<sup>6,8,15</sup>

In this paper we address the issue of suppression of

the ordered magnetic moment per Mn ion in manganite-based superlattices through measurements on  $\text{La}_{0.7}\text{Ca}_{0.3}\text{MnO}_3/\text{LaNiO}_3$  (LCMO/LNO) and  $\text{La}_{0.7}\text{Ca}_{0.3}\text{MnO}_3/\text{Er}_{0.7}\text{Sr}_{0.3}\text{MnO}_3$  (LCMO/ErSMO) systems. The choice of the spacer materials LNO and ErSMO, has been made on the basis of their nonmagnetic character, minimum lattice mismatch with LCMO and their diverse electrical behavior. Earlier measurements have shown  $\text{LaNiO}_3$  to be metallic<sup>20</sup> and  $\text{Er}_{0.7}\text{Sr}_{0.3}\text{MnO}_3$  an insulator down to 4.2 K.<sup>21</sup> In the LCMO/LNO system, we observe a  $\sim 20\%$  drop in moment when the spacer is very thin ( $\sim 1$  to 2 unit cells, u.c.). At this stage, the conductivity of the superlattices is dominated by a strain-related interfacial disorder. The moment per Mn ion quickly recovers its bulk value on increasing the spacer thickness. In the LCMO/ErSMO system, the moment per Mn ion of the magnetic layer (LCMO) shows a rapid drop followed by saturation at larger ErSMO thicknesses. From the magnetization data, we have extracted a critical distance  $\lambda_c$  from the interface over which the Mn-site spins are pinned by the stereochemical disorder, which arises presumably from distortions in the nearest neighbor environment of the Mn ions. While the  $\lambda_c$  attains saturation value in the LCMO/ErSMO system, in LCMO/LNO it tends to diminish as the spacer layer thickness is increased. Since LNO is metallic, this observation strongly suggests mobile-carrier-assisted depinning of the Mn spins in the critical zone.

A pulsed laser deposition system has been used for the growth of LCMO/LNO and LCMO/ErSMO multilayers on (001) oriented  $\text{LaAlO}_3$  substrates (lattice parameter  $a_0 = 3.792 \text{ \AA}$ ), which provides a low-lattice-mismatch surface for epitaxial growth. However, the constituent films are expected to be under compressive stress because of the negative lattice mismatch  $\Delta a \{=(a_0 - a_{\text{film}})/a_0\}$ , which for LCMO, LNO, and ErSMO is  $-1.8\%$ ,  $-0.9\%$ , and  $-0.7\%$ , respectively. The superlattices were synthesized by repeating 15 times the bilayers comprising of 20 u.c. LCMO and  $n$  u.c. LNO or ErSMO, with  $n$  taking values from 1 to 10. The periodicity of these structures was confirmed from the positions of superlattice reflections in x-ray  $\theta$ - $2\theta$  scans.<sup>21,22</sup> Most of the magnetization measurements were carried out at IIT-Kanpur using a superconducting quantum interference de-

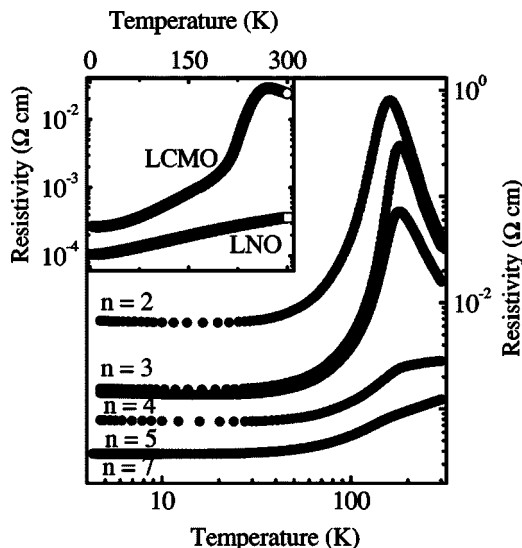


FIG. 1. Zero-field electrical resistivity  $\rho(T)$  of some  $(\text{La}_{0.7}\text{Ca}_{0.3}\text{MnO}_3)_m/(\text{LaNiO}_3)_n$  superlattices plotted as a function of temperature. A log-log scale has been used to emphasize the low-temperature behavior of the resistivity and the large changes in  $\rho(T)$  as the thickness of the spacer layer is increased. Inset shows the resistivity of LCMO and LNO films.

vice based magnetometer (Quantum Design—MPMS-5XL), with the magnetic field aligned along (010) direction in the plane of the superlattice. The resistivity of the samples was measured in the current-in-plane geometry.

In Fig. 1 shows the zero-field resistivity of some LCMO/LNO superlattices over the temperature window of 4.2 K to 300 K. As seen in the inset of the figure, a single layer film of  $\text{LaNiO}_3$  is metallic with a temperature dependence of the type  $\rho(T) = \rho_0 + \alpha T + \beta T^2$ , where the coefficients  $\rho_0$ ,  $\alpha$ , and  $\beta$  are  $1 \times 10^{-4} \Omega \text{ cm}$ ,  $4.18 \times 10^{-7} \Omega \text{ cm K}^{-1}$ , and  $1.648 \times 10^{-9} \Omega \text{ cm K}^{-2}$ , respectively. The resistivity of LCMO on cooling reaches a peak value at  $\sim 260 \text{ K}$ , followed by a precipitous drop and then a monotonic decrease down to 4.2 K. The low residual resistivity ( $\rho_0$ ), and the sharp peak at the Curie temperature  $T_c$  are indications of a good quality film.<sup>23</sup> For the lower values of  $n$ , the resistivity of the multilayers is dominated by the LCMO layers and by a disordered interfacial phase as discussed earlier<sup>22</sup> for the case of multilayers with 10 u.c. thick LCMO. These samples also show a large magnetoresistance at  $T < T_c$ . For higher values of  $n$  ( $\geq 4$ ), however, the current paths are shunted by the much more conducting LNO. A large drop in MR<sup>18,22</sup> and the disappearance of the peak in  $\rho(T)$  at  $T_c$  are indicative of this shunting.

The temperature dependence of electrical resistivity of the LCMO/ErSMO superlattices is shown in Fig. 2. Pure ErSMO is an insulator devoid of any FM or AF ordering down to the lowest temperature, as evident from the susceptibility vs temperature plot shown in the inset of Fig. 2 for a 2000 Å film. The resistivity of the superlattices with  $n > 7$  remain thermally activated down to the lowest temperature. However, the rise of  $\rho(T)$  is truncated below a critical temperature  $T^*$  which is lower than the Curie temperature  $T_c$  inferred from magnetization measurements. In fact, a quantification of magnetic ordering temperature from  $\rho(T)$  measurements

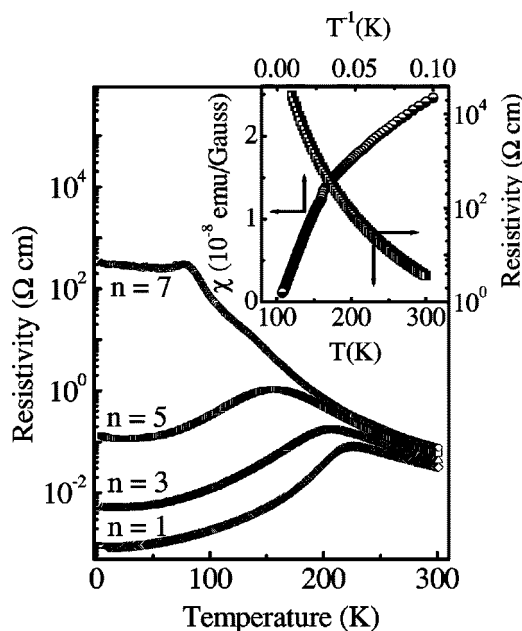


FIG. 2. Zero-field electrical resistivity  $\rho(T)$  of  $(\text{La}_{0.7}\text{Ca}_{0.3}\text{MnO}_3)_m/(\text{Er}_{0.7}\text{Sr}_{0.3}\text{MnO}_3)_n$  superlattices plotted as a function of temperature. Data for selected values of  $n$  are shown for the sake of clarity. Inset shows the resistivity and magnetic susceptibility of a 2000 Å thick  $\text{Er}_{0.7}\text{Sr}_{0.3}\text{MnO}_3$  deposited on (001)  $\text{LaAlO}_3$  substrate.

on these highly resistive samples is not free from ambiguity due to the percolative nature of transport in the disordered interfacial region of thickness  $\sim 25 \text{ Å}$ , as discussed in the following section. The  $\rho_0$  of these superlattices goes down dramatically and the  $T^*$  shifts up with the decreasing  $n$ . The behavior of resistivity displayed in Fig. 2 is typical of a manganite-based superlattice where the layers of a double-exchange-ferromagnet are separated by an insulator.<sup>6-9,12,15</sup> The dramatic increase in the low temperature resistivity with the thickness of ErSMO layers is accompanied by quenching of the magnetic moment of the LCMO layers. In Fig. 3 we show the zero-field-cooled  $M-H$  curves of some LCMO/LNO and LCMO/ErSMO superlattices taken at 10 K. The field dependence of magnetization in LCMO/ErSMO multilayers is remarkably different from that in the LCMO/LNO system. Here the remnant magnetization ( $M_r$ ) drops considerably even when the ErSMO layers are only 1 u.c. thick. This drop in  $M_r$  continues with the increasing  $n$ . We have also noticed that while the zero-field-cooled  $M-H$  loops of the samples are symmetric about the origin, the field-cooled loops show a shift towards the negative  $H$  axis.<sup>21</sup> This observation indicates exchange biasing<sup>9</sup> of the moments in LCMO. Interestingly, such effects are not seen in the case of LCMO/LNO where the spacer is a metal. Unlike the case of LCMO/LNO, the  $M-H$  loops of LCMO/ErSMO system also do not reveal a distinct saturation field ( $H_s$ ) and saturation moment ( $M_s$ ). We have extracted the  $M_s$  by extrapolating the linear part of the  $M-H$  curve to  $H=0$ . Similarly, the saturation field  $H_s$  has been identified as the field above which the magnetic moment approaches a linear field dependence.

If we attribute the  $M_s$  of the multilayers entirely to the Mn

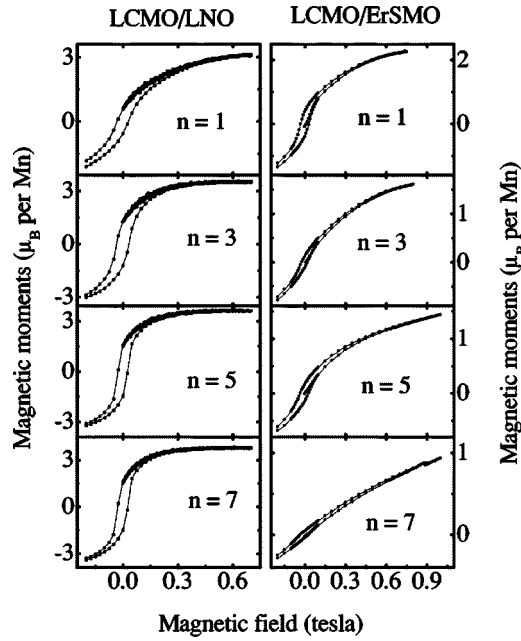


FIG. 3. Zero-field-cooled  $M$  vs  $H$  plots of the superlattices measured at 10 K. Only a small part of the negative branch of the loops is shown for the sake of clarity. The y axis is in units of Bohr magneton ( $\mu_B$ ) per Mn ions of the LCMO.

ions present in the LCMO, then the variation of moment per Mn ion with  $n$  is strikingly different for superlattices with the insulating and metallic spacers. As evident in Fig. 4, the  $M_s$  drops precipitously with  $n$  in the case of the former, whereas in the latter, the initial drop is followed by a quick recovery to

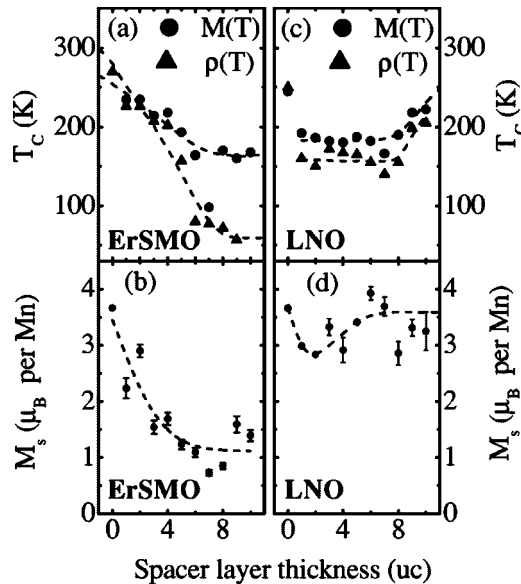


FIG. 4. Panels (a) and (c), respectively show the variation of  $T_c$  as a function of the spacer layer thickness. The critical temperature ( $T_c$ ) has been deduced from magnetization as well as resistivity measurements (the critical temperature deduced from resistivity measurements has been defined as  $T^*$  in the text). The variation of saturation moment per Mn ion for samples with ErSMO and LNO spacers is shown in panels (b) and (d), respectively.

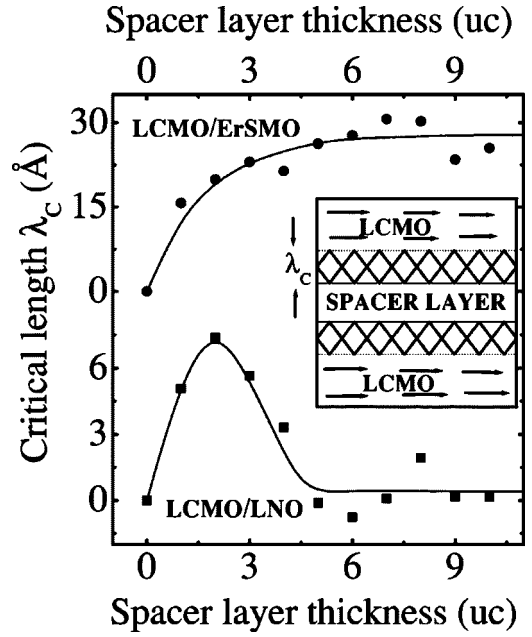


FIG. 5. Thickness ( $\lambda_c$ ) of the disordered interfacial zone is plotted as a function of the spacer layer thickness for the two types of superlattices. Inset shows a sketch of the disordered zone.

the bulk value for LCMO ( $\sim 3.7 \mu_B$ ). Figure 4 also shows the variation of  $T_c$  with  $n$ . A close resemblance is seen in the variation of  $T_c$  and  $M_s$  with  $n$  in both kinds of superlattices. While they continue to drop with the increasing  $n$  in LCMO/ErSMO, the initial drop is recovered in LCMO/LNO superlattices at the higher values of  $n$ . The quenching of magnetization per Mn ion of LCMO can be viewed as random pinning of the  $t_{2g}$  spins of each Mn site in the vicinity of the LCMO-spacer interfaces. The possible scenario is sketched in the inset of Fig. 5. The critical length scale ( $\lambda_c$ ) from the interface over which the Mn spins are frozen, has been calculated from the difference between the theoretical value of saturation magnetization per Mn ion in LCMO, and the measured saturation moment. Figure 5 shows the variation of  $\lambda_c$  with  $n$  in the two types of superlattices. The critical length in the case of ErSMO spacer first increases rapidly with  $n$ , and then reaches a saturation value of  $25 \text{ \AA}$  at  $n \sim 10$ . For the LNO spacer,  $\lambda_c$  peaks to  $\sim 7 \text{ \AA}$  at  $n=2$  and then decays to zero at  $n > 7$  within the uncertainty of these measurements. Here it needs to be emphasized that our calculation assumes an abrupt boundary between the pinned and free spins. The boundary, however, can be diffused. The result shown in Fig. 5 thus puts a lower bound on the thickness of the disordered region.

The most likely source of  $\lambda_c$  and its  $n$  dependence in LCMO/ErSMO superlattices is the interfacial disorder at various interfaces. Two possible mechanisms for such disorder can be identified. One is of a metallurgical origin where intermixing of the constituent elements of LCMO and the spacer takes place at the interfaces. However, x-ray diffraction and high-resolution transmission electron microscopy studies<sup>11,14,15,24-27</sup> on manganite and high  $T_c$  based superlattices reveal relatively sharp interfaces. While we have not undertaken a detailed study of the interfacial mixing, it is

expected to be negligible as our deposition conditions were similar to those used in studies where the interfaces have been analyzed in detail.<sup>11,15</sup> However, even an ideal termination can lead to four different kinds of interfaces between the films of two perovskites  $ABO_3$  and  $A'B'O_3$  grown along the (001) direction. For the case of LCMO-ErSMO system, these terminations are (i)  $MnO_2-La_{0.7}Ca_{0.3}O-Mn'O_2-Er_{0.7}Sr_{0.3}O$ , (ii)  $MnO_2-La_{0.7}Ca_{0.3}O-Er_{0.7}Sr_{0.3}O-Mn'O_2$ , (iii)  $La_{0.7}Ca_{0.3}O-MnO_2-Mn'O_2-Er_{0.7}Sr_{0.3}O$ , and (iv),  $La_{0.7}Ca_{0.3}O-MnO_2-Er_{0.7}Sr_{0.3}O-Mn'O_2$ , where  $Mn'$  represents the manganese ions of the ErSMO. While in configurations (i) and (ii) the Mn ions get their natural coordination, configurations (iii) and (iv) are far from being ideal. These changes in the nearest neighbor environment of the magnetic ions at interfaces, and modifications in bond angles and bond distances due to interfacial strain would lead to a disorder, which can be christened as stereochemical disorder. In metallic systems, such strain related disorder, which affects magnetic properties, has been identified as magnetic roughness.<sup>28,29</sup> The rapid increase followed by saturation of  $\lambda_c$  at  $n > 7$  in LCMO/ErSMO superlattices is consistent with this picture. Since the lattice parameters of ErSMO and LNO are very close ( $\Delta a \sim 0.1\%$ ), a similar behavior of  $\lambda_c$  should be expected in the case of LCMO/LNO superlattices. However, unlike ErSMO, LNO becomes highly metallic once its thickness increases beyond a few unit cells.<sup>22</sup> The presence of mobile carriers in the spacer and their motion across the interfaces is expected to enhance the coupling of Mn-site

spins in the disordered zone. Such carrier-assisted ordering of moments abounds in dilute metallic and semiconducting alloys with magnetic impurities.<sup>30,31</sup> This scenario also explains why a large quenching of the moment is seen in  $La_{0.6}Sr_{0.4}MnO_3/La_{0.6}Sr_{0.4}FeO_3$  (Ref. 7) and  $La_{0.6}Sr_{0.4}MnO_3/SrTiO_3$  (Ref. 15) superlattices where the spacer is poorly conducting, and the moment retains the bulk value of  $La_{0.6}Sr_{0.4}MnO_3$  in superlattices where the spacer ( $La_{0.45}Sr_{0.55}MnO_3$ ) is an antiferromagnetic metal.<sup>11</sup>

In summary, we have compared the changes in  $\rho(T)$ , magnetic ordering temperature and saturation moment of two  $La_{0.7}Ca_{0.3}MnO_3$ -based multilayers where the nonmagnetic spacer is a metal in one case and insulator in the other. The ordered moment per Mn ion of the ferromagnetic layers undergoes a giant quenching as the insulating spacer layer thickness is increased. Experiments suggest that the quenching is caused by pinning of the  $t_{2g}$  spins of Mn ions in the stereochemically disordered interfacial region of a critical thickness  $\lambda_c$ . We note that the quenching effects are not significant when the spacer layer is a metal, suggesting mobile carrier assisted depinning of the Mn-site spins in the disordered zone.

This research has been supported by a grant from the Department of Science and Technology, Government of India. The authors thank Dr. R. Lobo for some preliminary magnetization measurements.

<sup>1</sup>B. Y. Jin and J. B. Ketterson, *Adv. Phys.* **38**, 189 (1989).

<sup>2</sup>C. F. Majkrzak, D. Gibbs, P. Boni, A. I. Goldman, J. Kwo, M. Hong, T. C. Hsieh, R. M. Fleming, D. B. McWhan, Y. Yefet, J. W. Cable, J. Bohr, H. Grimm, and C. L. Chien, *J. Appl. Phys.* **63**, 3447 (1988).

<sup>3</sup>*Ultrathin Magnetic Structures I and II*, edited by B. Heinrich and J. A. C. Bland (Springer-Verlag, Berlin, 1994).

<sup>4</sup>G. Jacob, V. V. Moshchalkov, and Y. Bruynseraede, *Appl. Phys. Lett.* **66**, 2564 (1995).

<sup>5</sup>G. Q. Gong, A. Gupta, Gang Xiao, P. Lecoeur, and T. R. McGuire, *Phys. Rev. B* **54**, R3742 (1996).

<sup>6</sup>C. Kwon, K.-C. Kim, M. C. Robson, J. Y. Gu, M. Rajeswari, T. Venkatesan, and R. Ramesh, *J. Appl. Phys.* **81**, 4950 (1997).

<sup>7</sup>M. Izumi, Y. Murakami, Y. Konishi, T. Manako, M. Kawasaki, and Y. Tokura, *Phys. Rev. B* **60**, 1211 (1999).

<sup>8</sup>Moon-Ho Jo, Neil D. Mathur, Jan E. Evetts, Mark G. Blamire, Manuel Bibes, and Josep Fontcuberta, *Appl. Phys. Lett.* **75**, 3689 (1999).

<sup>9</sup>I. Panagiotopoulos, C. Christides, M. Pissas, and D. Niarchos, *Phys. Rev. B* **60**, 485 (1999).

<sup>10</sup>Kenji Ueda, Hitoshi Tabata, and Tomoji Kawai, *Phys. Rev. B* **60**, R12 561 (1999).

<sup>11</sup>M. Izumi, T. Manako, Y. Konishi, M. Kawasaki, and Y. Tokura, *Phys. Rev. B* **61**, 12 187 (2000).

<sup>12</sup>Yafeng Lu, J. Klein, C. Hofener, B. Wiedenhorst, J. B. Philipp, F. Herbstritt, A. Marx, L. Alf, and R. Gross, *Phys. Rev. B* **62**, 15 806 (2000).

<sup>13</sup>K. R. Nikolaev, A. Yu. Dobin, I. N. Krivorotov, W. K. Cooley, A. Bhattacharya, A. L. Kobrinskii, L. I. Glazman, R. M. Wentzovitch, E. Dan Dahlberg, and A. M. Goldman, *Phys. Rev. Lett.* **85**, 3728 (2000).

<sup>14</sup>H. Tanaka and T. Kawai, *J. Appl. Phys.* **88**, 1559 (2000).

<sup>15</sup>M. Izumi, Y. Ogimoto, Y. Okimoto, T. Manako, P. Ahmet, K. Nakajima, T. Chikyow, M. Kawasaki, and Y. Tokura, *Phys. Rev. B* **64**, 064429 (2001).

<sup>16</sup>A. Venimadhav, M. S. Hegde, R. Rawat, I. Das, P. L. Paulose, and E. Sampathkumaran, *Phys. Rev. B* **63**, 214404 (2001).

<sup>17</sup>Z. Sefrioui, D. Arias, V. Pena, J. E. Villegas, M. Verela, P. Prieto, C. Leon, J. L. Martinez, and J. Santamaria, *Phys. Rev. B* **67**, 214511 (2003).

<sup>18</sup>P. Padhan, R. C. Budhani, and R. P. S. M. Lobo, *Europhys. Lett.* **63**, 771 (2003).

<sup>19</sup>S. S. P. Parkin, N. More, and K. P. Roche, *Phys. Rev. Lett.* **64**, 2304 (1990).

<sup>20</sup>J. B. Goodenough, N. F. Mott, M. Pouchard, G. Demazeau, and P. Hagenmüller, *Mater. Res. Bull.* **8**, 647 (1973).

<sup>21</sup>P. Padhan, Ph.D. thesis, IIT-Kanpur, 2003.

<sup>22</sup>P. Padhan and R. C. Budhani, *Phys. Rev. B* **67**, 024414 (2003).

<sup>23</sup>P. Padhan, N. K. Pandey, S. Srivastava, R. K. Rakshit, V. N. Kulkarni, and R. C. Budhani, *Solid State Commun.* **117**, 27 (2001).

<sup>24</sup>Eric E. Fullerton, Ivan K. Schuller, H. Vanderstraeten, and Y. Bruynseraede, *Phys. Rev. B* **45**, 9292 (1992).

<sup>25</sup>J.-M. Triscone and Ø. Fischer, *Rep. Prog. Phys.* **60**, 1673 (1997).

- <sup>26</sup>C. B. Eom, A. F. Marshall, J.-M. Triscone, B. Wilkens, S. S. Laderman, and T. H. Geballe, *Science* **251**, 780 (1991).
- <sup>27</sup>F. Pailloux, D. Imhoff, T. Sikora, A. Barthelemy, J.-L. Maurice, J. P. Contour, C. Colliex, and A. Fert, *Phys. Rev. B* **66**, 014417 (2002).
- <sup>28</sup>Michael J. Pechan, J. F. Ankner, David M. Kelly, C. F. Majkrzak, and Ivan K. Schuller, *J. Appl. Phys.* **75**, 6178 (1994).
- <sup>29</sup>J. E. Mattson, C. H. Sowers, A. Berger, and S. D. Bader, *Phys. Rev. Lett.* **68**, 3252 (1992).
- <sup>30</sup>T. Deitl, H. Ohno, F. Matsukura, J. Cibert, and D. Ferrand, *Science* **287**, 1019 (2000).
- <sup>31</sup>Mona Berciu and R. N. Bhatt, *Phys. Rev. Lett.* **87**, 107203 (2001).